ACS APPLIED MATERIALS & INTERFACES

Letter

www.acsami.org

Osteogenic Commitment of Mesenchymal Stem Cells in Apatite Nanorod-Aligned Ceramics

Ying Chen,[†] Zhihui Sun,[‡] Yanyan Li,[‡] and Youliang Hong*[,†]

[†]National Engineering Research Center for Biomaterials, Sichuan University, Chengdu 610064, P. R. China

[‡]Department of Pharmacy of the First Hospital, Jilin University, Changchun 130012, P. R. China

Supporting Information

ABSTRACT: It is significant to process the clinically used biomaterials into a scaffold with specific nanotopographies, which can act as physical cues to regulate the osteogenic commitment of mesenchymal stem cells. In this study, hydroxyapatite (HAP) was considered as the processed objective and a facile, hydrothermal method was developed to grow the vertically oriented HAP nanorods in porous HAP ceramics. Experiments demonstrated that the formation of the HAP nanorods in porous ceramics was decided by a novel epitaxial growth mechanism and length of nanorods could be well-controlled by the growth time. Cell experiments demonstrated that such novel stereotopographical cues could regulate bone marrow mesenchymal stem cells to differentiate into the osteogenic lineage, thereby displaying that the porous ceramics with the HAP nanorods-aligned stereotopographies have a good prospect for applications in regenerative medicine of hard tissues.

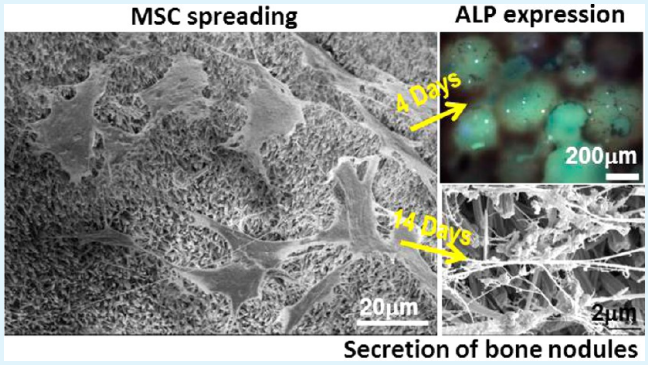

KEYWORDS: *apatite nanorods, mesenchymal stem cells, osteogenic commitment, regenerative medicine, mechanotransduction*

It is becoming an exciting research area in tissue engineering and regenerative medicine to design and fabricate biomaterials with specific signals to regulate the commitment of stem cells toward desirable lineage. To this end, a variety of biological, chemical, and physical strategies have been attempted, such as the incorporation of chemical/growth factors into biomaterial matrixes (e.g., BMP-2 is embedded into PLLA),[1] surface modification of biomaterials with functional groups (e.g., graft RGD on PLLA surface),[2] construction of special surface geometric feature,[3,4] topography and roughness,[5,6] modulation of substrate elasticity,[7,8] etc. Among these approaches, physical cues arisen from micro/nanoscale topography and roughness are particularly attractive because the micro/nanotopographies are cost-effective in comparison to expensive growth factors, and control nothing more than stem cell fate, not having in vivo variability and potential side effects.[9]

In the use of topographical cues to direct the fate decision of stem cells, recent studies have demonstrated that several kinds of micro/nanotopographies, including disordered pits,[5] pillars,[6] surface oriented nanotubes,[9] or nanowires,[10] could induce mesenchymal stem cells (MSCs), a kind of multipotent stem cells, to produce targeted osteogenic lineages. These findings would be very useful guidance, at the same time, also depicted good perspective for a range of applications in regenerative medicine of orthopedics and dentistry. Especially, because there are MSCs in bone marrow, MSCs can easily arrive at and interact with the topography of biomaterials implanted at the site of bone defect. Thus, the cost (including cell harvest and in vitro culture) and risk (e.g., immunologic rejection, mutation, etc.) of using the isolated cells can be eliminated completely.

Although the topographical cues have displayed striking advantages for orthopedic regenerative medicine, it still has a huge gap to translate this concept into clinical practices. At first, current success mainly is limited at two-dimensional (2D) models.[11] For practical clinical applications, however, three-dimensional (3D) stereoscaffolds will have to be used. The second obstacle is the preparation techniques. Current techniques, such as electron beam lithography,[12] photolithography,[13] soft lithography,[14] although can successfully construct specific micro/nanotopographies, such as pillars, groove, and pits, on 2D substrates, believed are difficult even impossible to achieve same topographies in 3D scaffolds, thereby it is still a complicated process associated with low repeatability and represents a challenge to fabricate the complex 3D biomedical scaffolds with nanoscale features.[15] Furthermore, most of the reported substrates for constructing nanotopographies, like silicon,[10] titanium,[16] and PMMA,[5] are nonsimilar in chemical components with hard tissues, and thus these nanotopographies are not optimal, even unsuitable for implanting into bone defects for hard tissue regeneration.

Received: September 22, 2014
Accepted: November 18, 2014
Published: November 18, 2014

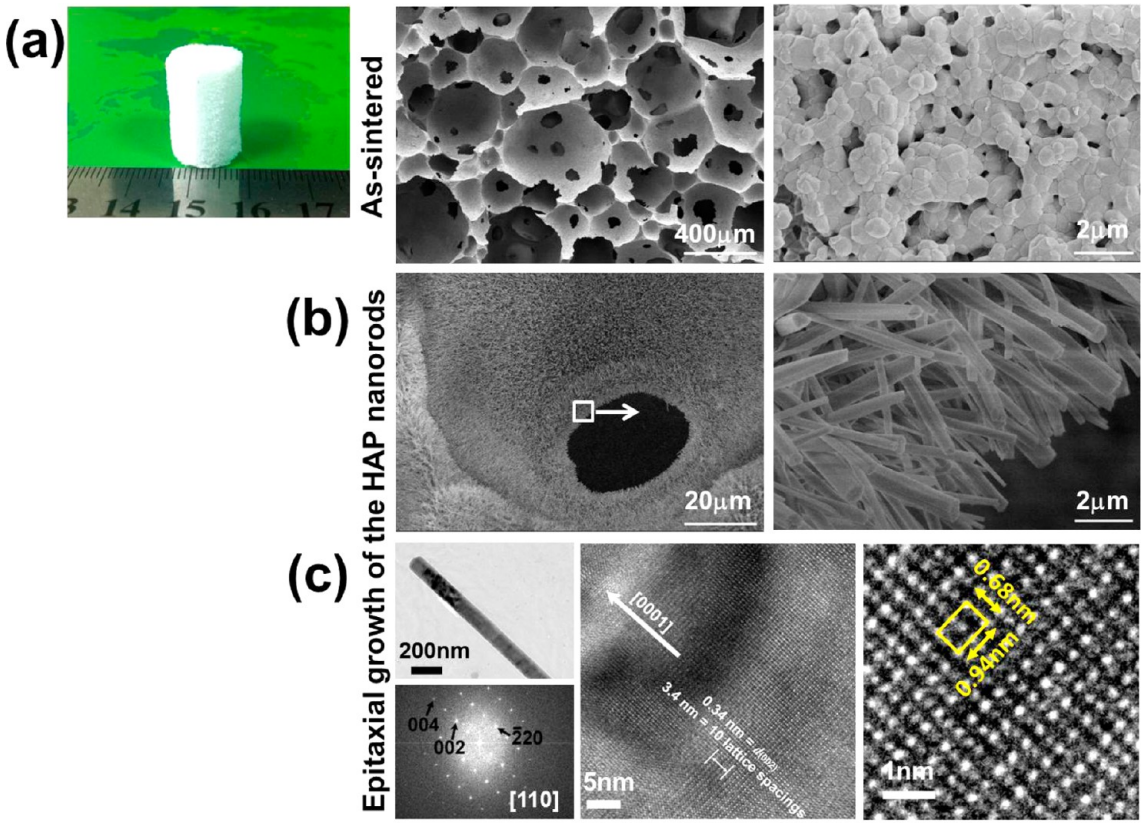

Figure 1. Preparation of the HAP nanorods-aligned ceramics. Porous HAP ceramic were (a) prepared at first as primary 3D structure, and then such ceramics were (b) used for epitaxial growth of the HAP nanorods on the surface of ceramics. (c) Ultrastructure of the grown HAP nanorod. Left top, middle, and right: low-, middle-, and high-magnification TEM image of the HAP nanorod; left bottom: FFT pattern of the HAP nanorod.

Herein we select hydroxyapatite (HAP, $Ca_{10}(PO4)_6(OH)_2$) as target materials to construct the HAP nanorod-aligned 3D nanotopographies by the epitaxial growth of the HAP nanorods in porous ceramics under a hydrothermal condition. HAP is considered because of its similarity in chemistry with mineral phase of human hard tissues, excellent biocompatibility, good bioactivity and osteoconductivity, and now HAP has been widely used as clinical materials in orthopedics. Once HAP is further tailored into 3D nanotopographies, such structural HAP scaffolds can be endowed with osteoinductivity because such nanotopographies can act as biophysical cues to mediate osteogenesis of MSCs through generating high cytoskeletal tension and activating the Rho A-initiating actin/myosin cytoskeletal contraction.[3] Thus, it could be very significant in hard tissue engineering, especially, it could be hopeful to extend the applications of HAP to guide the regeneration of large bone defectives.

To achieve the HAP nanorod-aligned 3D topographies, we prepared porous HAP ceramics at first as primary 3D structure. In a typical experiment, porous HAP ceramics were prepared by hydrogen peroxide gas foaming the HAP powders and subsequently sintering at air and at 1250 °C for 6 h, and the resulting cylindrical porous scaffold is shown in Figure 1a. Lowly magnified scanning electron microscopy (SEM) image shows that the as-prepared porous ceramic has abundant macropores with average pore diameter ∼310 μm, and these macropores are of interconnectivity. Highly magnified SEM image shows that the ceramic is composed of the HAP grains with average granule size ∼620 nm.

The as-sintered porous HAP ceramics then were reacted in an aqueous system containing ethylene diamine tetraacetic acid (EDTA), $Ca(NO_3)_2$ and $(NH_4)_2HPO_4$ (Ca/P: 1.67) under 150 °C hydrothermal condition for 24 h to the epitaxial growth of the HAP nanorods. Figure 1(b) shows that the hexagonal nanorods formed and vertically oriented toward macroporous substrates, and at the same time, the porous structures were remained. The average diameter and length of nanorods are 380 nm and length 17.5 μm, respectively (see Figure 2, 24 h). The ultrastructure of the grown HAP nanorods was examined by a high-resolution transmission electron microscopy (HR-TEM), and the results are shown in Figure 1(c). A fast Fourier transformation (FFT) pattern shows clear spots, corresponding to the [110] zone axis of the hexagonal structure with high crystallinity. The lattice parameters and axial angle determined for these patterns were $a = b = 0.94$ nm, $c = 0.68$ nm, and $a = b = 90°$, respectively, which are in good agreement with those of the HAP crystal structure. A middle- and high-magnification of the HR-TEM lattice image shows orthogonal linear lattices. The lattice spacing was determined to be 0.34 nm. The value is in good agreement with the $d(002)$. Highly magnified HR-TEM lattice image shows that the HAP crystal unit cell observed from the *a*,*b*-plane direction has a rectangular shape, which is 0.68 nm high and 0.94 nm long. In addition, these data also show that the [0001] crystallographic direction of the hexagonal HAP is parallel to the long axis of nanorod, indicating the HAP nanorods grew along the *c*-axis, i.e., growing vertically in the substrate of porous ceramics.

To fully understand the formation of nanorods, we carried out an investigation of their growth process over time, and the

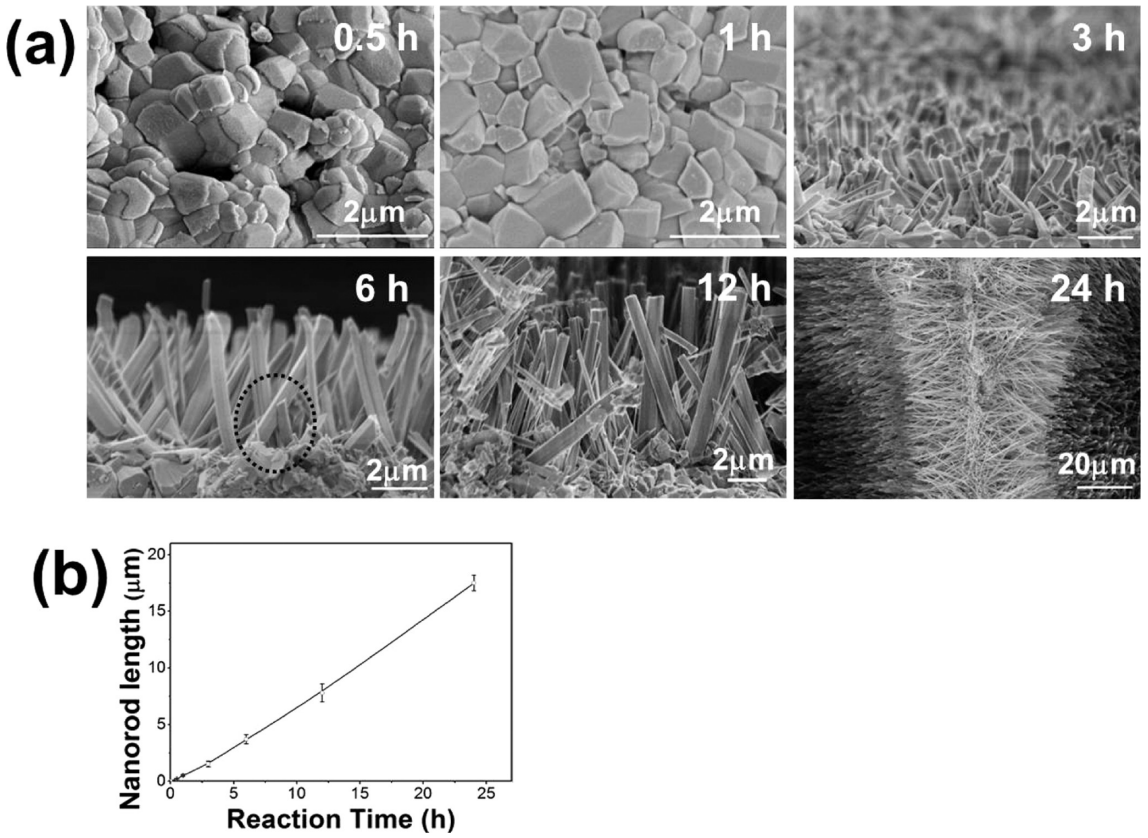

Figure 2. Growth of the HAP nanorods in porous ceramics over time. (a) SEM images of the HAP nanorods at different growth time. (b) Length of the HAP nanorods as a function of reaction time (mean ± s.d., n = 20).

results are shown in Figure 2. Interestingly, at initial stage (0.5 h), a layer of HAP fond of depositing on the *a*,*b*-planes of the substratal HAP grains trended to perfect the hexagonal structure of HAP. Presumably the reaction velocities of PO_4^{3-} and OH^- with the exposed Ca^{2+} on the *a*,*b*-planes (the *a*,*b*-planes are rich in Ca^{2+}) are far faster than that of the Ca-EDTA chelate complexes with the exposed PO_4^{3-} and OH^- on the *c*-plane (the *c*-plane is rich in PO_4^{3-} and OH^-),[17] which results in preferential deposition of HAP on the *a*,*b*-planes. After 1 h, perfect hexagonal structure almost formed, and these newly formed hexagonal HAP crystals succeeded to the crystallographic direction of the substratal HAP grains and were of random orientation. Additionally, the newly formed HAP nanorods show that their *a*,*b*-planes are smooth but the *c*-plane is rough (see 1 h), suggesting that active planes have converted from the *a*,*b*-planes to the *c*-plane and continuous growth of HAP along *c*-axis could occur. Subsequently, the length of nanorods continuously increased along *c*-axis in direct proportion to reaction time (Figure 2a, b). At the same time, the array of the HAP nanorods also changed gradually from random orientation to ordered alignment. The ordered alignment of nanorods can be attributed to geometrical selection process by exclusively eliminating the growth of crystals that are not optimally aligned, as can be seen from the dashed circle shown in the SEM image of 6 h.[18] Furthermore, no lateral and secondary nucleation was observed from the grown nanorods.

The formed HAP nanorods in the 3D HAP substrates, except the difference in dimensions, present many same/similar features with the substrate-oriented/aligned ZnO nanorods, especially, those synthesized from homoepitaxial substrate under hydrothermal condition,[18−21] including crystal structure (both are single crystal and belong to wurtzite hexagonal crystal system), growth direction (both grow along the *c*-axis), and the demand of seeds (The HAP grains were used for the growth of nanorods, and the homoepitaxial or heteroepitaxial seeds were used to induce the growth of the ZnO nanorods).[19−21] These same/similar features suggest that the growth process of the substrate-oriented/aligned ZnO nanorods could be shared to explain the formation mechanism of our HAP nanorods.[18] Still, our results indicated that the growth of the HAP nanorods is not completely same as the ZnO nanorods. At the initial stage, the growth of the HAP nanorods is extremely different from ZnO. The growth of the HAP nanorods on the HAP grains went through a transformation of from the *a*,*b*-planes to *c*-plane. In contrast, the ZnO nanorods would grow directly following most thermodynamically stable crystal habit of the seeds deposited on substrates.[18−21]

In addition, our results show that the substrates with 3D structure hardly affect the growth and vertical orientation of the HAP nanorods. It can be understood because the curvature of macropores at micro/nanoscale is very small, as can be seen from Figure 2, which may be approximated as 2D plane at micro/nanoscale and has a little effect on geometrical selection during the growth of nanorods at a relatively short period of time (e.g., within 24 h).

The HAP nanorod-aligned porous ceramics prepared from the 24 h hydrothermal reaction subsequently were used to culture with bone marrow MSCs (BM-MSCs) of neonatal rabbits. Then, alkaline phosphatase (ALP) activity and biomineralization of BM-MSCs cultured in the HAP nanorod-aligned ceramics were monitored to make sure whether

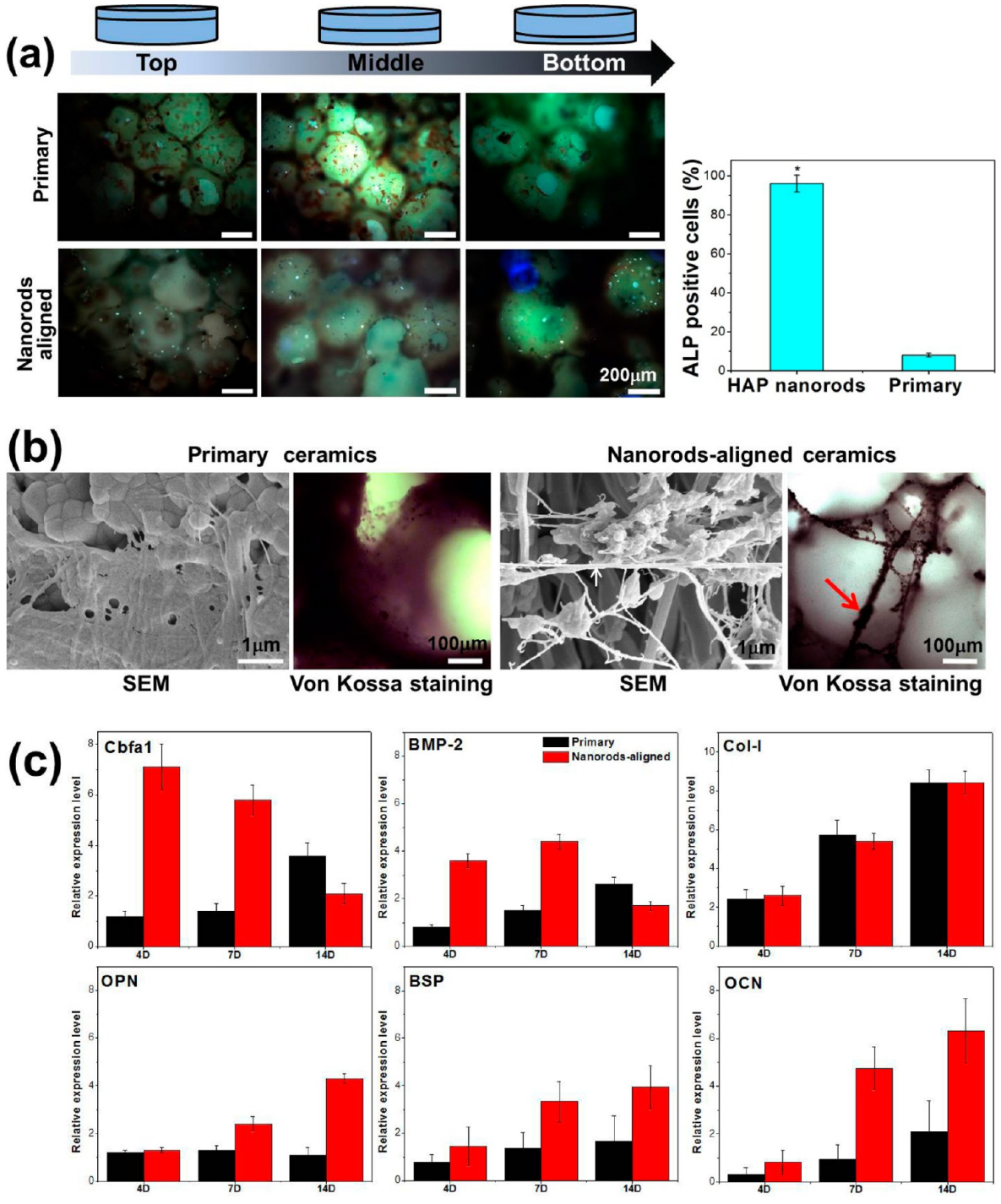

Figure 3. Osteogenic commitment of MSCs. (a) ALP staining and quantification of ALP expression of MSCs cultured in the HAP nanorods-aligned and primary porous ceramics at day 4 (means ± s.d.). (b) SEM images and Von Kossa staining show that the MSCs cultured in porous ceramics with the aligned HAP nanorods for 14 days expressed abundant mineral nodules, but not in primary porous ceramic. (c) PCR of cells cultured in samples over time.

BM-MSCs would commit toward osteogenic lineages. ALP is detected because ALP is a potent and significant predictor of osteogenic lineage commitment, and also is a highly specific marker and inducer of bone formation.[22] Very interestingly, at day 4, ALP was expressed by cells throughout ceramic, as shown in Figure 3a (bright dots in ceramics). Figure 3a further shows that the expressed ALP is very high (96%). Besides ALP, another specific marker of osteogenic differentiation, mineral nodules secreted by the cells cultured in the nanorods-aligned ceramics for 14 days, also were demonstrated by Von Kossa staining. As can be seen from Figure 3b, these extracellular matrixes contained the secreted mineral granules (e.g., black granules embedded in filament matrix denoted by red arrow). SEM observation (Figure 3b) further demonstrated the expression of mineral nodules. For comparison, primary porous ceramics were used to culture with BM-MSCs as a control. Figure 3a shows that ALP hardly was expressed by cells at day

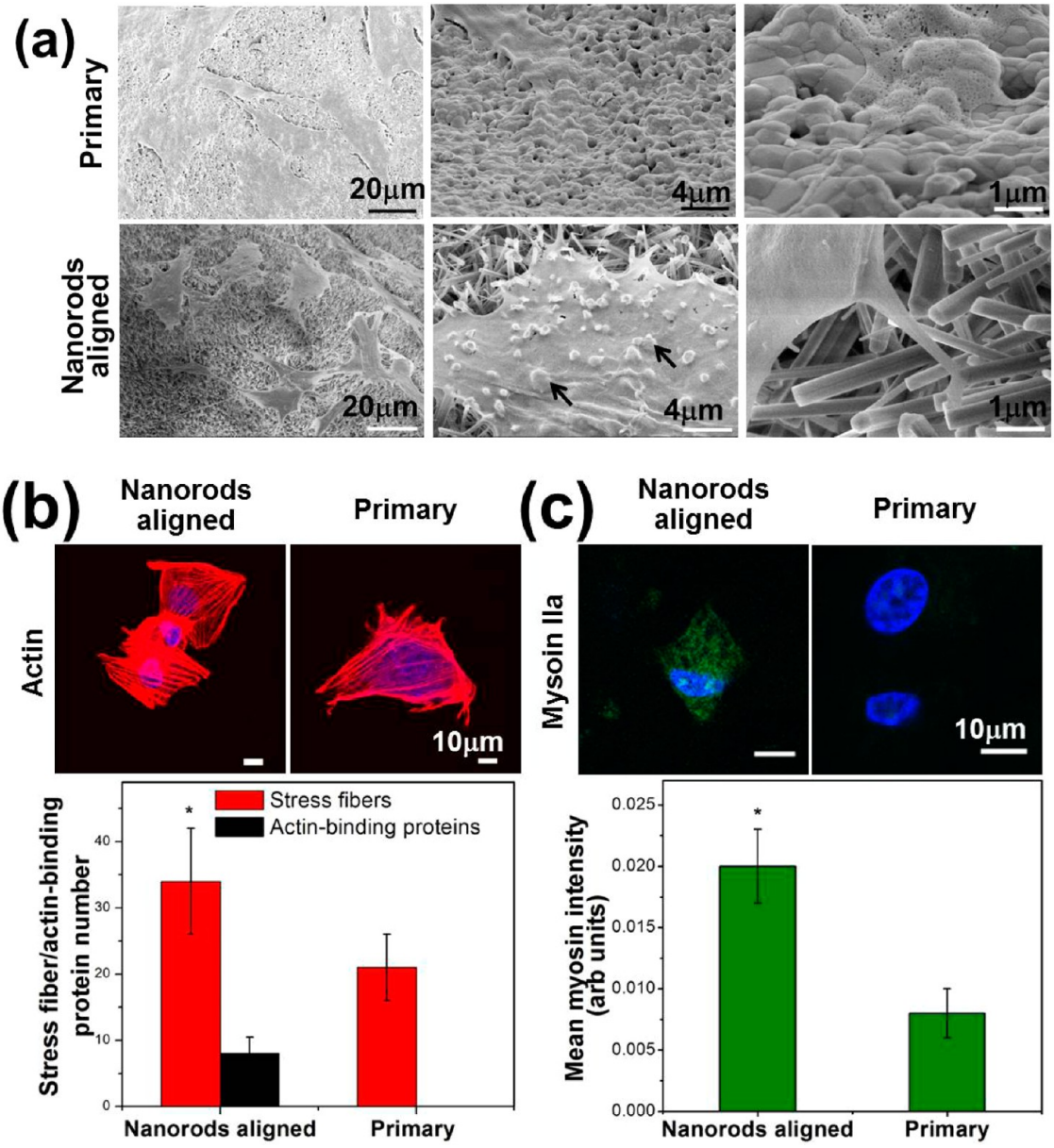

Figure 4. Spreading and cytoskeletal organization of MSCs. (a) SEM images, (b) phalloidin staining for F-actin, and (c) immunoflurescent staining for myosin IIa in the nanorod-aligned and primary HAP ceramics show that MSCs have significantly larger contractile tension after 3 days of culture (mean ± s.d., $n = 20$; * $p < 0.05$, t-test).

4, and SEM and Von Kossa staining (Figure 3b) show that no mineral nodules were secreted by cells.

Furthermore, a real-time polymerase chain reaction (RT-PCR) was used to test the osteogenic gene expressions of MSCs cultured in two kinds of samples over time. As shown in Figure 3c, Cbfa1, a maker of early osteoblastic differentiation, was expressed highly by cells at the nanorods-aligned topographies at day 4 and then decreased at day 14. By comparison, in primary ceramics the expression of Cbfa1 by cells was low at day 4 but increased slightly at day 14. Still, the expression level at day 14 in primary ceramics was lower than that in the topographies at day 4. Similar tendency also occurred at BMP-2. Nevertheless, the expression level of BMP-2 in the topographies arrived at maximum value at day 7. Different from Cbfa1 and BMP-2, the expression of Col-I was similar in both samples, i.e., the expression of Col-I increased gradually over time and the expression level was also similar as each other. OPN, late osteogenic makers, was expressed by cells in topographies at day 7 and was increased at day 14, but was not expressed by cells in primary ceramics in the whole culture time. Another two kinds of the mineral-relative genes, BSP and OCN,[23,24] both were expressed highly in the nanorods-aligned ceramics at later stage but both expressions were weak in primary ceramics. Such results well-verified the formation of mineral nodules as shown in Figure 3b. Especially, because OCN can be only expressed by osteoblasts,[29] the MSCs adhered in the HAP nanorod-aligned topographies surely have differentiated into osteoblasts.

Taken together, these direct evidence, i.e., the expression of abundant ALP, mineral nodules, and osteogenic gene expressions well-verified the osteogenic differentiation of BM-MSCs induced by the HAP nanorods-constructed 3D topographies. The MSCs cultured in the nanorod-constructed topographies could be induced into osteoblasts and the process

of MSCs' osteogenic commitment was associated with but faster than the model of osteoblastic differentiation.[25] Primary HAP ceramics did not mediate osteogenic differentiation of MSCs within a short culture period, and the distinctive biofunctional difference of two kinds of ceramics, obviously, can be attributed to the HAP nanorods-constructed topographies.

Now it has been well-known that topographies have an essential role in regulation of cell adhesion, and some specific topographies, as described above, even can induce MSCs to osteogenesis. It is considered that transmembrane adhesion receptors of the integrin family have a primary role in regulating stem cell function. The underlying mechanism of osteogenesis from MSCs in response to topographies is that the cell-generated traction forces resulted from topographies trigger contraction-driving Rho A kinase (ROCK), which is central to the derivation of the high tensional state required for osteogenesis through activation of Rho A-initiating actin/myosin cytoskeletal contraction.[3,26] Still, because different topographies reported are associated with different structures, the manner in which topographies cause cells to generate cytoskeleton tension is not same completely. For example, Dalby group has verified that the PMMA-constructed, irregularly arrayed nanopits could directly induce a significant cellular tension for osteogenesis,[5] but the regularly arrayed ones could not.[27] It suggested that a small difference in topographies even could change the behaviors of MSCs.

Also, the osteogenesis of MSCs in the HAP nanorod-constructed topographies suggests that MSCs adopted a different adhesive manner on the HAP nanorod-aligned surface in comparison with primary ceramics. To verify such speculation, we carried out the experiments of cell adhesion in primary and the HAP nanorod-aligned ceramics. SEM images (Figure 4a) shows that after 4 days of culture BM-MSCs could fully spread in nanotopographies and presented a strong adhesive tension. The middle-magnification of SEM image shows that in microscale area, some small filopodia adhered/wrapped around nanorods and abundant nanoimprintings (black arrows) of nanorods in lamellae could be observed. Highly magnified SEM image further shows that filopodia could anchor on both the *c*-plane and the *a*,*b*-planes, indicating the adhesion is nonspecific. Phalloidin staining shows that BM-MSCs could well assemble a cortical F-actin cytoskeleton throughout cytoplasm and actin-binding proteins between parallel actin filaments (Figure 4b, Figure S2 in the Supporting Information showed the magnified picture to indicate the actin-binding proteins). These assembled stress fibers presented were under the stretched state.

On the substrate surface of primary ceramics, Figure 4a shows that MSCs also could spread well on the surface of porous walls and phalloidin staining (Figure 4b) indicates the concentrated actin filaments. Nevertheless, no actin-binding proteins were observed and Figure 4b shows that cells assembled significantly less actin filaments compared to MSCs in the nanorod-aligned topographies.

Furthermore, another kind of actin-binding motor protein, nonmuscle myosin IIa, that binds and cross-links actin filaments and then mediates sliding of antiparallel actin filaments during contraction of stress fibers and thereby increasing endogenous cell tension,[22,28,29] also were investigated. The immunofluorescence staining clearly indicates that high-levels of myosin IIa were expressed in the nanorod-aligned topographies, whereas low levels of myosin IIa were expressed in primary ceramic.

Taken together, above results clearly show that it is the nanorods-aligned topographies rather than primary ceramics that could drive cells to assemble myosin IIa and generate a strong contractile force. Especially, the emergence of visible actin-binding proteins (Figure 4b) indicates that the nanorod-aligned topographies could cause cells to form higher level of intracellular tension than on these reported topographies, thus promoting the osteogenesis of MSCs.

Hence, the spreading of MSCs in primary ceramic indicates that primary ceramic is a compliant substrate, in which substrate stiffness just drives cells to organize cytoskeleton to keep an adhesion/tension balance. The MSCs adhered on such compliant substrate could not promote the organized cytoskeletal filaments to generate a high-enough tensed cytoskeletal force to trigger the assembly of myosin IIa. In the HAP nanorod-aligned ceramics, however, besides substrate stiffness, the well-oriented HAP nanorods provided sites for cell adhering and stretching to expand initial adhesion spots and for initiating nanoimprintings, which could allow the spread cells to strongly contract, thereby triggering strong contractility of myosin IIa and then activating downstream Rho-ROCK signal pathway.[3]

In addition, the osteogenic differentiation of MSCs shown here well demonstrates that topographies are available not only on 2D substrates, but also in 3D structures. In fact, our macropores have so large diameter as to render the curvature of macropores small with respect to a single cell, as can been seen from Figure 4a, the individual cells spread on the substrates of pore wall are quite flat. Therefore, the curvature of macropores postulated has little effect on mediating the commitment of MSCs. Nevertheless, after cells were continuously cultured for another 7 days, cells proliferated extremely and filled up porosities (see Figure S3 in the Supporting Information). It shows that such porosities play key roles in mediating 3D organization of cells (2D substrates cannot) and allow further spatial pattering of cells, i.e., morphogenesis,[30] to form bone tissues.

In summary, the 3D HAP nanotopographies constructed by the well-aligned HAP nanorods were successfully fabricated by novel epitaxial growth of the HAP nanorods in porous HAP ceramics under hydrothermal conduction. The growth process of the HAP nanorods in the HAP substrates went through a preferential deposition of HAP on the *a*,*b*-planes of the substratal HAP grains at first, then a growth transformation of from the *a*,*b*-planes to the *c*-plane, and last continuous growth along *c*-axis. Such stereonanotopographies demonstrated alone could regulate MSCs to differentiate into osteogenic lineages. Achieving such osteoinductive 3D nanotopographies extremely shortens the gap of from the concept of mechanotransduction, i.e., extracellular physical forces sponsored from materials features can be converted into chemical signals to alter the fate decision of MSCs, to clinical applications. Especially, because the fabrication of such nanotopographies is simple, repeatable, and low-cost, and the tailored materials, HAPs, do not contain the elements that human body does not have, and now have been widely used in clinical practice, the 3D HAP nanotopographies reported here depict a good prospect for a range of applications in regenerative medicine of hard tissues.

■ ASSOCIATED CONTENT

Supporting Information

The outcomes of the 21-day cell culture in the nanorod-aligned topographies. This material is available free of charge via the Internet at http://pubs.acs.org.

■ AUTHOR INFORMATION

Corresponding Author

*E-mail: hyl@scu.edu.cn.

Author Contributions

Y.C. conducted the synthesis of the 3D scaffolds. Z.S. and Y.L. carried out the biological experiments. Y.H. developed the concept, supervised the project, conceived the experiments, and wrote the manuscript.

Funding

This work was supported by National Natural Science Foundation of China (Grant 31170928).

Notes

The authors declare no competing financial interest.

■ ABBREVIATIONS

2D, two-dimensional
3D, three-dimensional
HAP, hydroxyapatite
ALP, alkaline phosphatase
MSCs, mesenchymal stem cells
BM-MSCs, bone marrow- mesenchymal stem cells
BMP-2, bone morphogenetic protein-2
PLLA, poly-L-lactide
RGD, arginine-glycine-aspartate acid
SEM, scanning electron microscopy
HR-TEM, high-resolution transmission electron microscopy
FFT, fast Fourier transformation
EDTA, ethylene diamine tetraacetic acid

■ REFERENCES

(1) Li, J.; Hong, J.; Zheng, Q.; Guo, X.; Lan, S.; Cui, F.; Pan, H.; Zou, Z.; Chen, C. Repair of Rat Cranial Bone Defects with nHAC/PLLA and BMP-2-Related Peptide or rhBMP-2. *J. Orthop. Res.* **2011**, *29*, 1745−1752.

(2) Alvarez-Barreto, J. F.; Landy, B.; VanGordon, S.; Place, L.; DeAngelis, P. L.; Sikavitsas, V. I. Enhanced Osteoblastic Differentiation of Mesenchymal Stem Cells Seeded in RGD-Functionalized PLLA Scaffolds and Cultured in A Flow Perfusion Bioreactor. *J. Tissue Eng. Regener. Med.* **2011**, *5*, 464−475.

(3) McBeath, R.; Pirone, D. M.; Nelson, C. M.; Bhadriraju, K.; Chen, C. S. Cell Shape, Cytoskeletal Tension, and RhoA Regulate Stem Cell Lineage Commitment. *Dev. Cell* **2004**, *6*, 483−495.

(4) Kilian, K. A.; Bugarija, B.; Lahn, B. T.; Mrksich, M. Geometric Cues for Directing the Differentiation of Mesenchymal Stem Cells. *Proc. Natl. Acad. Sci. U.S.A.* **2010**, *107*, 4872−4877.

(5) Dalby, M. J.; Gadegaard, N.; Tare, R.; Andar, A.; Riehle, M. O.; Herzyk, P.; Wilkinson, C. D. W.; Oreffo, R. O. C. The Control of Human Mesenchymal Cell Differentiation Using Nanoscale Symmetry and Disorder. *Nat. Mater.* **2007**, *6*, 997−1003.

(6) Sjöström, T.; Dalby, M. J.; Hart, A.; Tare, R.; Oreffo, R. O.C.; Su, B. Fabrication of Pillar-Like Titania Nanostructures on Titanium and Their Interactions with Human Skeletal Stem Cells. *Acta Biomater.* **2009**, *5*, 1433−1441.

(7) Discher, D. E.; Janmey, P.; Wang, Y. Tissue Cells Feel and Respond to the Stiffness of Their Substrate. *Science* **2005**, *310*, 11393−11343.

(8) Engler, A. J.; Sen, S.; Sweeney, H. L.; Discher, D. E. Matrix Elasticity Directs Stem Cell Lineage Specification. *Cell* **2006**, *126*, 677−689.

(9) Oh, S.; Brammer, K. S.; Li, Y. S. J.; Teng, D.; Engler, A. J.; Chien, S.; Jin, S. Stem Cell Fate Dictated Solely by Altered Nanotube Dimension. *Proc. Natl. Acad. Sci. U.S.A.* **2009**, *106*, 2130−2135.

(10) Kuo, S. W.; Lin, H. I.; Ho, J. H. C.; Shih, Y. R. V.; Chen, H. F.; Yen, T. J.; Lee, O. K. Regulation of The Fate of Human Mesenchymal Stem Cells by Mechanical and Stereo-Topographical Cues Provided by Silicon Nanowires. *Biomaterials* **2012**, *33*, 5013−5022.

(11) Ross, A. M.; Jiang, Z.; Bastmeyer, M.; Lahann, J. Physical Aspects of Cell Culture Substrates: Topography, Roughness, and Elasticity. *Small* **2012**, *8*, 336−355.

(12) Hatakeyama, H.; Kikuchi, A.; Yamato, M.; Okano, T. Patterned Biofunctional Designs of Thermoresponsive Surfaces for Spatiotemporally Controlled Cell Adhesion, Growth, and Thermally Induced Detachment. *Biomaterials* **2007**, *28*, 3632−3643.

(13) Molna, P.; Wang, W. S.; Natarajan, A.; Rumsey, J. W.; Hickman, J. J. Photolithographic Patterning of C2C12 Myotubes Using Vitronectin as Growth Substrate in Serum-Free Medium. *Biotechnol. Prog.* **2007**, *23*, 265−268.

(14) Whitesides, G. M.; Ostuni, E.; Takayama, S.; jiang, X. Y.; Ingber, D. E. Soft Lithography in Biology and Biochemistry. *Annu. Rev. Biomed. Eng.* **2001**, *3*, 335−373.

(15) Biggs, M. J. P.; Richards, R. G.; Dalby, M. J. Nanotopographical Modification: A Regulator of Cellular Function through Focal Adhesions. *Nanomedicine* **2010**, *6*, 619−633.

(16) Sjöström, T.; McNamara, L. E.; Dominic Meek, R. M.; Dalby, M. J.; Su, B. 2D and 3D Nanopatterning of Titanium for Enhancing Osteoinduction of Stem Cells at Implant Surfaces. *Adv. Healthcare Mater.* **2013**, *2*, 1285−1293.

(17) Zhuang, Z.; Fujimi, T. J.; Nakamura, M.; Konishi, T.; Yoshimura, H.; Aizawa, M. Development of a,b-plane-Oriented Hydroxyapatite Ceramics as Models for Living Bones and Their Cell Adhesion Behavior. *Acta Biomater.* **2013**, *9*, 6732−6740.

(18) Chernov, A. A.; Drabek, B. A.; Satcher, J. J. H.; Han, T. Y. J. Experimental Validation of the Geometrical Selection Model for Hydrothermally Grown Zinc Oxide Nanowire Arrays. *Chem. Mater.* **2013**, *25*, 1363−1371.

(19) Tak, Y.; Yong, K. Controlled Growth of Well-Aligned ZnO Nanorod Array Using a Novel Solution Method. *J. Phys. Chem. B* **2005**, *109*, 19263−19269.

(20) Greene, L. E.; Law, M.; Tan, D. H.; Montano, M.; Goldberger, J.; Somorjai, G.; Yang, P. General Route to Vertical ZnO Nanowire Arrays Using Textured ZnO Seeds. *Nano Lett.* **2005**, *5*, 1231−1236.

(21) Wu, W.; Hu, G.; Cui, S.; Zhou, Y.; Wu, H. Epitaxy of Vertical ZnO Nanorod Arrays on Highly (001)-Oriented ZnO Seed Monolayer by a Hydrothermal Route. *Cryst. Growth Des.* **2008**, *8*, 4014−4020.

(22) Parsons, J. T.; Horwitz, A. R.; Schwartz, M. A. Cell Adhesion: Integrating Cytoskeletal Dynamics and Cellular Tension. *Nat. Rev. Mol. Cell Biol.* **2010**, *11*, 633−643.

(23) Hunter, G. K.; Goldberg, H. A. Nucleation of hydroxyapatite by bone sialoprotein. *Proc. Natl. Acad. Sci. U.S.A.* **1993**, *90*, 8562−8565.

(24) Ducy, P.; Desbois, C.; Boyce, B.; Pinero, G.; Story, B.; Dunstan, C.; Smith, E.; Bonadio, J.; Goldstein, S.; Gundberg, C.; Bradley, A.; Karsenty, G. Increased bone formation in osteocalcin-deficient mice. *Nature* **1996**, *382*, 448−452.

(25) Stein, G. S.; Lian, J. B. Molecular mechanisms mediating proliferation/differentiation interrelationships during progressive development of the osteoblast phenotype. *Endocr. Rev.* **1993**, *14*, 424−442.

(26) Tsimbouri, P. M.; McMurray, R. J.; Burgess, K. V.; Alakpa, E. V.; Reynolds, P. M.; Murawski, K.; Kingham, E.; Oreffo, R. O. C.; Gadegaard, N.; Dalby, M. J. Using Nanotopography and Metabolomics to Identify Biochemical Effectors of Multipotency. *ACS Nano* **2102**, *6*, 10239−10249.

(27) McMurray, R. J.; Gadegaard, N.; Tsimbouri, P. M.; Burgess, K. V.; McNamara, L. E.; Tare, R.; Murawski, K.; Kingham, E.; Oreffo, R.

O. C.; Dalby, M. J. Nanoscale surfaces for the long-term maintenance of mesenchymal stem cell phenotype and multipotency. *Nat. Mater.* **2011**, *10*, 637−644.
(28) Meili, R.; Latorre, B. A.; del Álamo, J. C.; Firtel, R. A.; Lasheras, J. C. Myosin II Is Essential for the Spatiotemporal Organization of Traction Forces during Cell Motility. *Mol. Biol. Cell* **2010**, *21*, 405−417.
(29) Manzanares, M. V.; Ma, X.; Adelstein, R. S.; Horwitz, A. R. Non-Muscle Myosin II Takes Centre Stage in Cell Adhesion and Migration. *Nat. Rev. Mol. Cell Biol.* **2009**, *10*, 778−790.
(30) Purnell, B. A. Getting into Shape. *Science* **2013**, *340*, 1183.